

Towards controllable Si-doping in oxide molecular beam epitaxy using a solid SiO source: Application to β -Ga₂O₃

A. Ardenghi^{1*}, O. Bierwagen^{1*}, A. Falkenstein², G. Hoffmann¹, J. Lähnemann¹, M. Martin², P. Mazzolini^{3*}

¹ Paul-Drude-Institut für Festkörperelektronik, Leibniz-Institut im Forschungsverbund Berlin e.V., Hausvogteiplatz 5-7, 10117 Berlin, Germany

² Institute of Physical Chemistry, RWTH Aachen University, D-52056 Aachen, Germany

³ Department of Mathematical, Physical and Computer Sciences, University of Parma, Viale delle Scienze 7/A, 43124 Parma, Italy

*Email: ardenghi@pdi-berlin.de - bierwagen@pdi-berlin.de - piero.mazzolini@unipr.it

The oxidation-related issues in controlling Si doping from the Si source material in oxide molecular beam epitaxy (MBE) is addressed by using its solid suboxide, SiO, as an alternative source material in a conventional effusion cell. Line-of-sight quadrupole mass spectrometry of the direct SiO-flux (Φ_{SiO}) from the source at different temperatures (T_{SiO}) confirmed SiO molecules to sublime with an activation energy of 3.3eV. The T_{SiO} -dependent Φ_{SiO} was measured in vacuum before and after subjecting the source material to an O₂-background of 10⁻⁵ mbar (typical oxide MBE regime). The absence of a significant Φ_{SiO} difference indicates negligible source oxidation in molecular O₂. Mounted in an oxygen plasma-assisted MBE, Si-doped β -Ga₂O₃ layers were grown using this source. The Φ_{SiO} at the substrate was evaluated [from 2.9x10⁹cm⁻²s⁻¹ (T_{SiO} =700°C) to 5.5x10¹³cm⁻²s⁻¹ (T_{SiO} =1000°C)] and Si-concentration in the β -Ga₂O₃ layers measured by secondary ion mass spectrometry highlighting unprecedented control of continuous Si-doping for oxide MBE, *i.e.*, N_{Si} from 4x10¹⁷cm⁻³ (T_{SiO} =700°C) up to 1.7x10²⁰cm⁻³ (T_{SiO} =900°C). For a homoepitaxial β -Ga₂O₃ layer an Hall charge carrier concentration of 3x10¹⁹cm⁻³ in line with the provided Φ_{SiO} (T_{SiO} =800°C) is demonstrated. No SiO-incorporation difference was found between β -Ga₂O₃(010) layers homoepitaxially grown at 750°C and β -Ga₂O₃(-201) layers heteroepitaxially grown at 550°C. However, the presence of activated oxygen (plasma) resulted in partial source oxidation and related decrease of doping concentration (particularly at T_{SiO} <800°C) which has been tentatively explained with a simple model. Degassing the source at 1100°C reverted the oxidation. Concepts to reduce source oxidation during MBE-growth are referenced.

THE MANUSCRIPT

Due to a high variety of functional properties, metal oxides are rising in popularity as material systems for innovative optoelectronic devices.¹ Among metal oxides monoclinic β -Ga₂O₃ is one of the most interesting ones, and it has been particularly intensely investigated in the past decade.² In fact, due to a predicted breakdown field around 8 MV/cm as a

consequence of its bandgap of about 4.8 eV, β -Ga₂O₃ is one of the most promising novel materials for power electronics.³ Moreover, it can be grown from the melt^{4–7} in turn allowing for β -Ga₂O₃ homoepitaxy of high quality layers.³

To obtain a broad range of devices for power electronic application, a thorough control on the electrical properties is needed.⁸ Considering the lack of *p*-type doping for Ga₂O₃,⁹ the main focus is on the group-IV elements in order to tune *n*-type doping. So far, Ge, Si and Sn have been already successfully employed as dopants in homoepitaxial layers grown with different technique such as Molecular Beam Epitaxy (MBE),^{5,10–15} Metal Organic Chemical Vapor Deposition (MOCVD)^{16–19} and Metal Organic Vapor Phase Epitaxy (MOVPE)^{20,21}.

Lany has theoretically shown²² that Si can be considered as a better donor compared to Ge and Sn, since it is predicted to be the only truly shallow donor among them. From a survey of experimental data collected on semiconducting, homoepitaxial β -Ga₂O₃ layers,⁸ the highest electron mobilities μ over a broad range of electron concentrations n are achieved with Si or Ge doping; the generally lower μ in Sn-doped films is likely related to a deep donor state identified for Sn.¹² Controlled Si doping in β -Ga₂O₃ has been already demonstrated in MOCVD but not in MBE. This is most likely linked to the two limitations of Si doping in MBE systems.

The first one is due to the unintentional incorporation of Si, probably related to the quartz cavity of the plasma source in oxygen plasma-assisted MBE (PAMBE)^{23,24} and is limiting the low concentration side of the doping window ($N_{\text{Si}} < 10^{18} \text{ cm}^{-3}$).

The second one is due to instable Si-doping concentration in PAMBE-grown Ga₂O₃ layers, that depend on the oxygen background pressure rather than the Si source temperature as pointed out by Kalarickal *et al.*,¹³ As underlying process, they identified the oxidation of the elemental Si source resulting in the source flux to consist of the SiO suboxide which has a higher vapor pressure than Si. Further oxidation of the Si surface into solid SiO₂ was identified by Krishnamoorthy *et al.*¹⁵ to cause drastic flux reduction during layer growth due to the lower vapor pressure of SiO₂.

Indeed, the oxidation of the heated elemental source in an oxygen background into its volatile suboxide happens for many elements, including In, Ga, Ge, or Sn.²⁵ This can rule either the Ge- or Sn-doping of oxides (including in the Ga₂O₃ material system), or the growth rates for Ga₂O₃ during MBE deposition at relatively low Ga-source temperatures (*e.g.* <750 °C). Despite similar suboxides formation, the use of a Sn-metal source for Ga₂O₃ in PAMBE is more controllable with respect to a Si one,¹² but can involve segregation problems.²⁶ For Ge-doping of Ga₂O₃ from a Ge-source in PAMBE, an additional strong dependence of doping concentration on T_g has been shown.¹⁴ High concentrations ($N_{\text{Ge}} \approx 10^{20} \text{ cm}^{-3}$) required relatively low T_g (600°C), potentially placing limits on the crystal quality of the deposited layers.

An efficient solution to control Si doping in oxide MBE while avoiding massive oxidation of the source, could be the use of an oxide or suboxide source material in the cell,²⁷ similar to the use of SnO_2 , SnO , or mixtures of Sn and SnO_2 to produce a SnO flux,^{26,28} or mixtures of Ga and Ga_2O_3 to produce a Ga_2O flux.^{28,29} Major advantages in the use of a suboxide (or mixed elemental+oxide) sources over an oxide one are the significantly lower cell temperatures required and the absence of parasitic oxygen formation.²⁸ On the other hand, controllable Si doping would benefit from a SiO_2 source that cannot oxidize further as SiO could. Based on the vapor pressure of SiO_2 ,²⁷ the geometry of our growth chamber, and the temperature limit of conventionally employed effusion cells (1200 °C), however, the Si concentration in layers deposited at a typical growth rate of 4.5 nm/min would be limited to $N_{\text{Si}} \leq 10^{19} \text{ cm}^{-3}$. For example, a high-temperature effusion cell run at $T_{\text{SiO}_2}=1400$ °C would be required to obtain $N_{\text{Si}} = 1 \times 10^{20} \text{ cm}^{-3}$ (considering that a GR of 1 Å/s in our MBE system correlate to a partial pressure of the source material in the effusion cell on the order of 10^{-3} mbar ²⁸).

In comparison, a SiO source could reach $N_{\text{Si}} = 1.7 \times 10^{20} \text{ cm}^{-3}$ at $T_{\text{SiO}}=900$ °C, which prompted us to characterize a solid SiO source for PAMBE growth with a focus on doping $\beta\text{-Ga}_2\text{O}_3$ layers. In particular, we demonstrate the possibility to obtain Si-doping concentrations on a wide range - from $4 \times 10^{17} \text{ cm}^{-3}$ (limited by the background Si concentration in the PAMBE deposited layers) up to $1.7 \times 10^{20} \text{ cm}^{-3}$ - in both homoepitaxial and heteroepitaxial $\beta\text{-Ga}_2\text{O}_3$ layers, with negligible dependence on the growth orientation and/or the growth temperature. For our study, an Al_2O_3 crucible loaded with 10 g of 3-6 mm SiO lumps (4N purity, Alfa Aesar) was placed in a conventional single-filament effusion cell.

At first, we characterized the direct flux from this SiO source using a quadrupole mass spectrometer (QMS) mounted line in sight to the cell inside a custom build system which is schematically shown in the inset of [Figure 1](#) and described in Ref. ²⁸. The composition of the flux from the SiO source at a base pressure in the low 10^{-8} mbar regime is reported in [Figure 1 \(a\)](#) for a cell temperature of $T_{\text{SiO}} = 1200$ °C chosen to maximize the signal-to-noise ratio for the identification of the different desorbing species. Due to the natural abundance of stable isotopes of Si at 28 amu (92.23%), 29 amu (4.67%), and 30 amu (3.1%), the major signals shown in [Figure 1 \(a\)](#) can be clearly identified as SiO . A weaker Si signal is recorded and related to fragmentation inside the QMS.²⁸ To remove interference with residual N_2 (having the same mass per charge as ^{28}Si) the measurements with closed cell shutter were subtracted from those with opened shutter. The same qualitative SiO spectra could be recorded down to $T_{\text{SiO}} = 880$ °C where the ^{44}SiO signal reaches the noise level.

To calculate the activation energy E_a for SiO sublimation, the ^{44}SiO signal was recorded at T_{SiO} ranging from 1200 °C to 800 °C in vacuum. The corresponding Arrhenius plot yields $E_a = 3.29 \text{ eV}$ (red line in [Figure 1 \(b\)](#)) in good agreement with the $E_a = 3.41 \text{ eV}$ (black line in [Figure 1 \(b\)](#)) extracted from the thermodynamic calculation of Adkison²⁷.

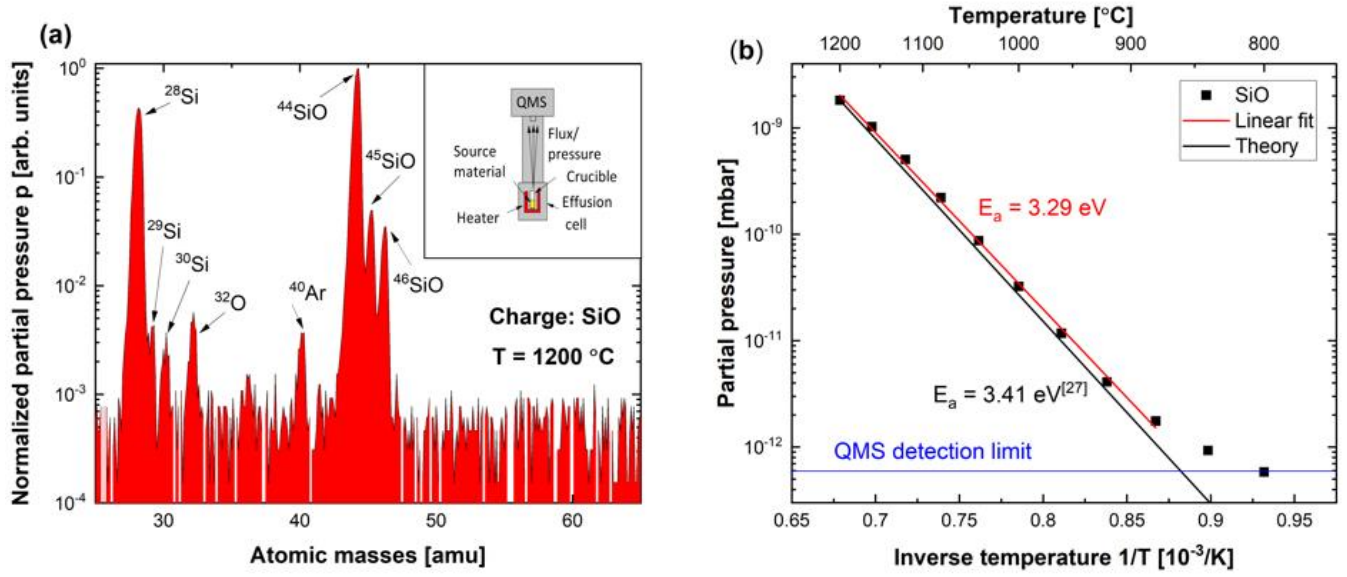


Figure 1 (a) QMS spectrum (red) of the flux from the SiO cell at $T=1200$ °C in vacuum. Inset: Sketch of the system used for the measurement. (b) Arrhenius plot of the SiO signals collected in vacuum (black squares) for the experimental determination of the activation energy in comparison to the extrapolated activation energy from theory²⁷ (red and black lines, respectively).

To investigate potential source oxidation in molecular oxygen, the source was exposed to a controlled O_2 background of $p = 1 \times 10^{-5}$ mbar (typical for PAMBE growths) for periods of 30–180 minutes at various T_{SiO} . A potential surface oxidation to SiO_2 during this exposure is expected to reduce the SiO flux (Φ_{SiO}) with respect to the untreated SiO source material. Figure 2 shows the comparison of the measured SiO partial pressure during the ramp up (performed in vacuum) from $T_{\text{SiO}}=700$ °C to 1200 °C before and after exposure of the source to an O_2 background pressure of 1×10^{-5} mbar for 3 h at $T_{\text{SiO}}=700$ °C. The matching partial pressure recorded in both experiments indicate that the SiO source did not get oxidized. The initial (up to 15 min) higher values detected for the SiO partial pressure after the oxidation process (red dashed lines in Figure 2) are due to the higher background pressure caused by residual oxygen in the chamber after the treatment.

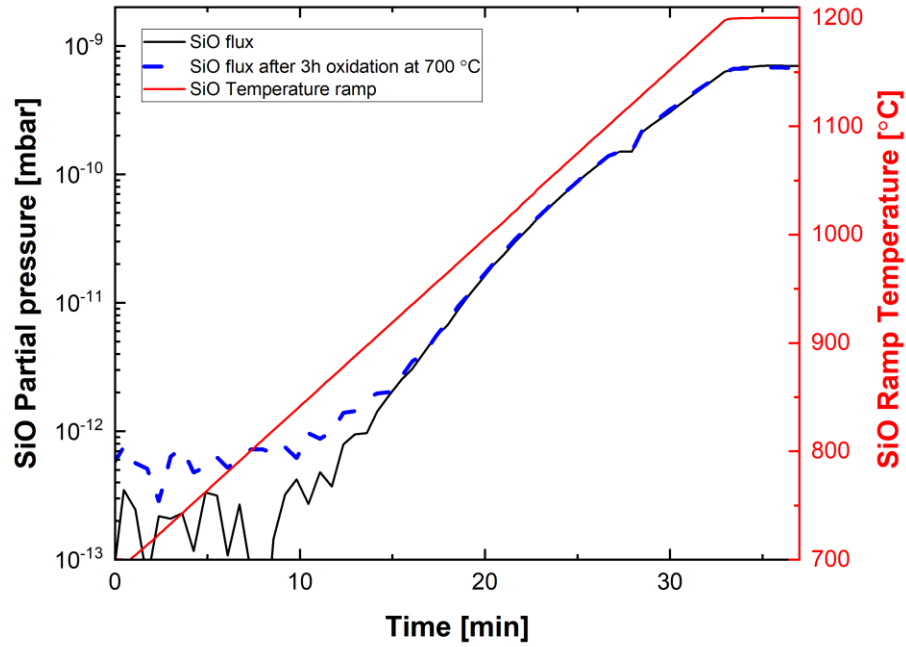


Figure 2 Partial pressure from the SiO source for a ramp from 400 °C to 1200 °C before oxidation (black solid line) and after 3h with molecular oxygen background $p = 10^{-5}$ mbar at $T_{\text{SiO}} = 700$ °C (red dashed line). After the 3h at $p = 10^{-5}$ mbar the O-flow was closed and the chamber was pumped down to $p = 5 \times 10^{-8}$ mbar. The source was then ramped up at 1200 °C.

Next, the crucible with the SiO source material was mounted in our PAMBE growth chamber for doping experiments. In order to predict the SiO-flux and consequential Si doping concentration in MBE deposited $\beta\text{-Ga}_2\text{O}_3$ layers as a function of the T_{SiO} , we extrapolated the corresponding Φ_{SiO} for $T_{\text{SiO}} = 1000^\circ\text{C}$ ($\Phi_{\text{SiO}}^{1000^\circ\text{C}} = 5.5 \times 10^{13} \text{ cm}^{-2} \text{ s}^{-1}$) towards lower T_{SiO} . $\Phi_{\text{SiO}}^{1000^\circ\text{C}}$ was extracted from the growth rate of an amorphous SiO_2 layer as described in the supplementary material.

$$\Phi_{\text{SiO}}(T) = \Phi_{\text{SiO}}^{1000^\circ\text{C}} e^{[-E_a(1/kT - 1/k1000^\circ\text{C})]}. \quad (1)$$

Eq. (1) provides this extrapolation, shown as the solid line in Figure 3, using the activation energy E_a from the QMS experiment [red line in Figure 1 (b)]. Knowing the $\beta\text{-Ga}_2\text{O}_3$ growth rate - in our case a typical value is $GR_{\text{Ga}_2\text{O}_3} = 4.5 \text{ nm/min}$ - it is possible to derive the expected Si doping concentration, e.g., $N_{\text{Si}} = 7.3 \times 10^{21} \text{ cm}^{-3}$ for $T_{\text{SiO}} = 1000$ °C using:

$$N_{\text{Si}} = \frac{\Phi_{\text{SiO}}(T)}{GR_{\text{Ga}_2\text{O}_3}}. \quad (2)$$

The predicted values obtained from Eq. (1) and Eq. (2) were used as our guideline to investigate different doping concentrations in $\beta\text{-Ga}_2\text{O}_3$ layers both on $\text{Al}_2\text{O}_3(0001)$ and $\beta\text{-Ga}_2\text{O}_3(010)$ substrates grown at T_g of 550 °C and 750 °C, respectively (see

supplementary material). Depth profiles of the Si dopant were obtained by time-of-flight secondary ion mass spectrometry (ToF-SIMS IV, iontof GmbH, Germany). For quantification, the relative sensitivity factor for silicon in a gallium oxide matrix was obtained by measuring an implantation standard of Si implanted into a nominally undoped β -Ga₂O₃ single crystal with a 10^{14} cm⁻² fluence and an implantation energy of 80 keV.

In Figure 3 symbols represent the different ϕ_{SiO} at the substrate as function of the corresponding T_{SiO} , calculated as the product of N_{Si} (measured by SIMS) and $GR_{\text{Ga}_2\text{O}_3}$ (obtained from SIMS profile) following Eq. 2. For reference, the corresponding volumetric Si concentrations are shown assuming a fixed growth rate of 4.5 nm/min (average GR of the deposited samples) on the right y-scale of Figure 3. The obtained broad range of Si doping concentrations from $3\text{--}4 \times 10^{17}$ cm⁻³ ($T_{\text{SiO}} = 700$ °C) up to 1.7×10^{20} cm⁻³ ($T_{\text{SiO}} = 900$ °C) demonstrates the possibility to use a SiO source charge for continuous doping in β -Ga₂O₃ thin films controlled by the source temperature in PAMBE. Nonetheless, it was not possible to demonstrate the possibility of achieving doping concentrations below 3×10^{17} cm⁻³ due to an unintentional Si-doping in the nominally undoped β -Ga₂O₃ layers of around 2×10^{17} cm⁻³ detected by SIMS. We tentatively relate this unintentional Si incorporation to the plasma source as recently pointed out by Asel *et.al.*²⁴

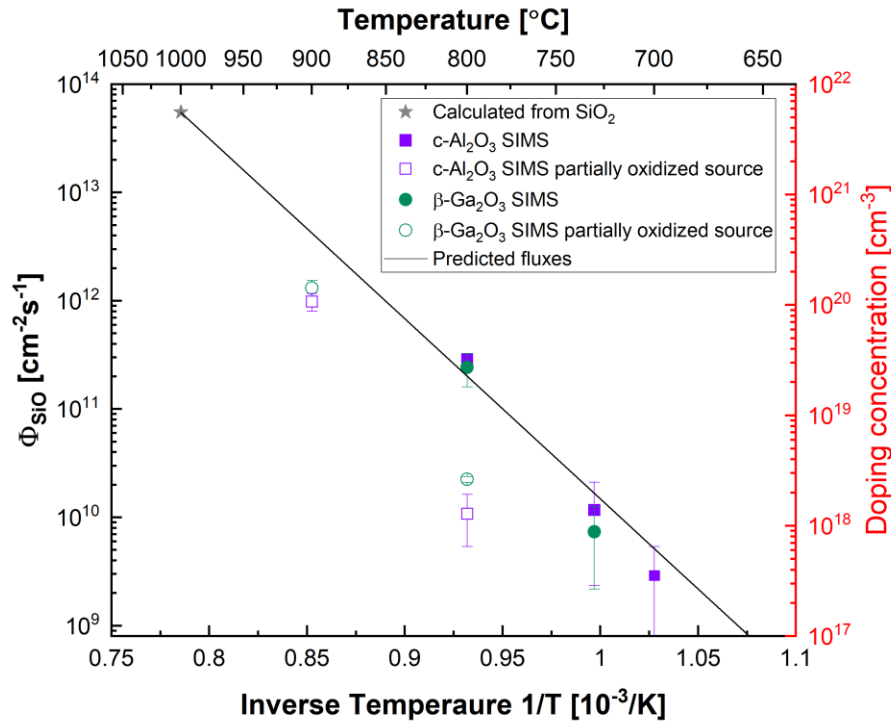


Figure 3 SiO flux at the substrate as a function of the T_{SiO} ; the right red scale shows the doping concentration considering a fixed β -Ga₂O₃ GR of 4.5 nm/min. Empty points are referred to layers grown with a partially oxidized source. For the filled ones, the SiO cell was ramp up at $T_{\text{SiO}} = 1100$ °C before the deposition (dwell $t = 30$ min) in order to restore the SiO cell before the growth. The error bars represent the variation in the doping concentration along the layer thickness with respect to its average concentration. The solid black line refers to the extrapolated SiO flux calculated using Eq.1.

A close inspection of the Si doping profiles of all the deposited $\beta\text{-Ga}_2\text{O}_3$ films reveals a systematically decreasing Si concentration towards the surface, as exemplarily shown in Figure 4 (a). The respective highest and lowest Si concentrations from the begin and end of the doped layers are reflected by the corresponding error bars in Figure 3. Before the growth of the doped layers, the SiO cell was kept at the corresponding temperature for 15-60 min, in order to exclude the thermalization of the source as the possible origin of the slope. Consequently, we attribute the decreasing Si concentration in the doping profiles to progressive oxidation of the surface of the source material into SiO_2 during PAMBE growth. This finding is just apparently in contrast to the absence of source oxidation in molecular oxygen (see Figure 2), since it confirms the findings of Kalarickal et al.¹³ who suggested active oxygen to play a major role for the oxidation of the Si source into SiO_2 in PAMBE. To further understand the impact of source oxidation, two different data set are provided in Figure 3. The empty symbols mark samples grown with a partially oxidized source, while the filled ones show data for samples where a high temperature cycle ($T_{\text{SiO}}=1100$ °C, 30-60 min) was carried out before the layer growth to degas and restore the SiO surface. At $T_{\text{SiO}}=800$ °C, the comparison between the two sets of data leads to a difference around one order of magnitude for the Φ_{SiO} (cf. Figure 3). Notwithstanding, the Si concentrations from the begin of the layers grown with a freshly degassed cell (upper error bar of filled symbols in Figure 3) follow the vapor pressure behavior of SiO, confirming the principal control of Si-doping by the source temperature rather than the background pressure. In addition, the matching incorporated SiO-flux concentration at the same T_{SiO} both on (0001) Al_2O_3 ($T_g = 550^\circ\text{C}$) and $\beta\text{-Ga}_2\text{O}_3$ ($T_g = 750^\circ\text{C}$), strongly suggests (i) a negligible dependence of Si-incorporation on the T_g as was instead observed for Ge,¹⁴ and (ii) a negligible dependence on the $\beta\text{-Ga}_2\text{O}_3$ growth orientation [*i.e.*, (-201) and (010), respectively].

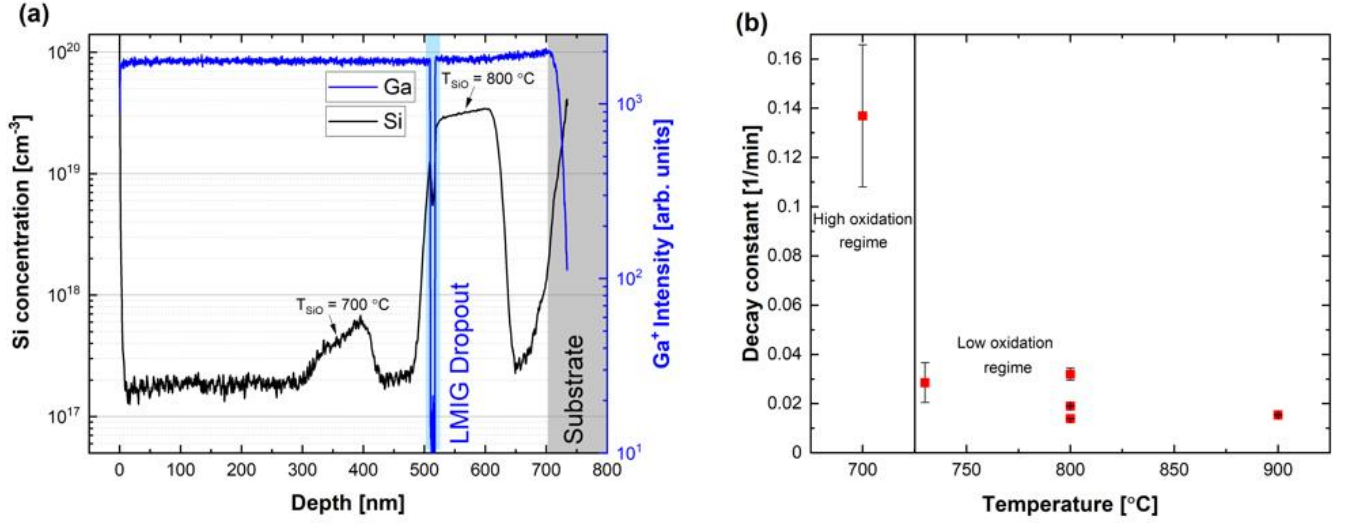


Figure 4 (a) SIMS doping profile for a β - Ga_2O_3 sample grown with different T_{SiO} . The drop of the signal around 500 nm is caused by a dropout of the liquid metal ion gun (LMIG). A slope in the profile is visible, showing a steeper slope at lower T_{SiO} . (b) Decay constant calculated from a linear fit of the SIMS profile in log scale. Before the fitting the Si background was subtracted and used to calculate the error bar. The error bars highlight how the background subtraction become important, *i.e.* how close the measured concentration is with respect to the background level (defined for nominally undoped layers).

Further inspection of [Figure 4 \(a\)](#) suggests the slope of the decreasing Si-concentration to depend on the SiO cell temperature, being steeper for a $T_{\text{SiO}} = 700$ °C compared to the one at 800 °C. In a simple oxidation model (pictorially explained in the supplementary material, Fig. S2), the unoxidized area of the source material decreases with a rate constant λ . Consequently, an exponentially decreasing Φ_{SiO} (which is proportional to this area) is expected during source oxidation:

$$\Phi_{\text{SiO}}(t) = \Phi_{\text{SiO}}(0)e^{-\lambda \cdot t} \quad (3)$$

where $\Phi_{\text{SiO}}(0)$ corresponds to the flux at $t=0$. Using [Eq. 3](#), [Eq. 2](#), and the relation of layer thickness d and corresponding growth time t ($d = GR_{\text{Ga}_2\text{O}_3} t$), we extracted λ from the slopes of the SIMS profiles $d(\ln N_{\text{Si}})/d(d)$ as:

$$\lambda = GR_{\text{Ga}_2\text{O}_3} d(\ln N_{\text{Si}})/d(d) \quad (4)$$

[Figure 4 \(b\)](#) shows the extracted λ for layers doped at different T_{SiO} and suggests two different oxidation regimes: (i) for a $T_{\text{SiO}} > 730$ °C an almost flat doping profiles signify a low rate constant, (ii) for lower T_{SiO} , a high λ indicates non-stable doping throughout the layer thickness (*e.g.*, decrease in the doping concentration from $6.8 \times 10^{17} \text{ cm}^{-3}$ down to $2 \times 10^{17} \text{ cm}^{-3}$ in a deposition time $t=15$ min, *i.e.* over a 90 nm layer thickness). These data suggest lower T_{SiO} (within the investigated range) to promote oxidation of the source, similar to the observations of Kim *et al.* for the Sr source oxidation.³⁰

Finally, room temperature Van der Pauw-Hall measurements (details in supplementary material) were performed on a homoepitaxially grown sample with a 124 nm-thick Si-doped layer ($N_{Si} = 3 \times 10^{19} \text{ cm}^{-3}$). The extracted Hall electron concentration of $n = 3 \times 10^{19} \text{ cm}^{-3}$ with an electron mobility μ of $25 \text{ cm}^2/\text{Vs}$ and a sheet resistance R_s of $645 \text{ }\Omega/\text{sq}$ confirms effective Si-doping by our approach perfectly in line with the provided Φ_{SiO} .

In conclusion, we have demonstrated the potential of a solid SiO source to provide a wide range of SiO fluxes controlled by the source temperature of a conventional effusion cell. Using this source, SiO fluxes at the substrate ranging from 5.5×10^{13} ($T_{SiO}=1000 \text{ }^\circ\text{C}$) to 2.9×10^9 ($T_{SiO}=700 \text{ }^\circ\text{C}$) $\text{cm}^{-2}\text{s}^{-1}$ were used to grow a SiO_2 layer as well as continuously Si doping $\beta\text{-Ga}_2\text{O}_3$ layers with concentrations ranging from 1.7×10^{20} ($T_{SiO}=900 \text{ }^\circ\text{C}$) cm^{-3} to 3×10^{17} ($T_{SiO}=700 \text{ }^\circ\text{C}$) cm^{-3} inside an oxide PAMBE. Hall measurements of a homoepitaxial Si-doped $\beta\text{-Ga}_2\text{O}_3$ layer deposited with a T_{SiO} corresponding to an expected $N_{Si} = 3 \times 10^{19} \text{ cm}^{-3}$ (800°C) revealed the same charge carrier density ($n = 3 \times 10^{19} \text{ cm}^{-3}$) indicating effective doping. The Si-incorporation did not depend on substrate temperature (550°C , 750°C) or the Ga_2O_3 growth orientation [(010), (-201)].

An oxidation of the SiO source, leading to a decreasing SiO flux, has been observed in active oxygen (plasma) but not in molecular oxygen at similar background pressures. The decreasing flux has been parametrized by a decay constant λ , extracted from the measured Si-doping profiles. Our initial data indicates a strong oxidation regime ($\lambda \geq 0.14 \text{ min}^{-1}$) for relatively low T_{SiO} ($\leq 730 \text{ }^\circ\text{C}$) and a milder one ($\lambda < 0.015 \text{ min}^{-1}$) at higher T_{SiO} ($\geq 800 \text{ }^\circ\text{C}$). The partial oxidation of the source can be reproducibly reverted by degassing at $T_{SiO} = 1100 \text{ }^\circ\text{C}$.

We believe that our approach can be also applied to O_3 -MBE as well as for doping of other oxides, *e.g.* In_2O_3 . Suggested ways to reduce the source oxidation during growth by oxygen PAMBE include (i) an increased T_{SiO} or (ii) a decreased activated oxygen p_{O_2} at the SiO source. The (i) can be realized by a modified source geometry, *e.g.*, using an aperture on the crucible³¹ or an increased source-to-substrate distance,³⁰ to necessitate a higher SiO vapor pressure (and thus higher T_{SiO}) inside the crucible to obtain the same SiO flux at the substrate. The (ii) can be realized using growth conditions that require less oxygen,³² *e.g.*, metal-exchange catalyzed MBE (MEXCAT-MBE),^{33–36} or a differentially pumped SiO source.³⁷

Acknowledgments:

We would like to thank Duc Van Dinh for critically reading the manuscript, as well as Hans-Peter Schönherr, Claudia Herrmann, Carsten Stemmler, and Steffen Behnke for their technical support on the MBE and test chamber. This work was performed in the framework of GraFOx, a Leibniz-ScienceCampus, and was funded by Deutsche Forschungsgemeinschaft (DFG, German Research Foundation) - project number 446185170.

Data Availability:

The data that support the findings of this study are available from the corresponding author upon reasonable request

References:

- ¹ X. Yu, T.J. Marks, and A. Facchetti, [Nat. Mater.](#) **15**, 383 (2016).
- ² S.J. Pearton, J. Yang, P.H. Cary, F. Ren, J. Kim, M.J. Tadjer, and M.A. Mastro, [Appl. Phys. Rev.](#) **5**, 011301 (2018).
- ³ M. Higashiwaki, K. Sasaki, A. Kuramata, T. Masui, and S. Yamakoshi, [Appl. Phys. Lett.](#) **100**, 013504 (2012).
- ⁴ Z. Galazka, R. Uecker, D. Klimm, K. Irmscher, M. Naumann, M. Pietsch, A. Kwasniewski, R. Bertram, S. Ganschow, and M. Bickermann, [ECS J. Solid State Sci. Technol.](#) **6**, Q3007 (2017).
- ⁵ A. Kuramata, K. Koshi, S. Watanabe, Y. Yamaoka, T. Masui, and S. Yamakoshi, [Jpn. J. Appl. Phys.](#) **55**, 1202A2 (2016).
- ⁶ E. Ohba, T. Kobayashi, T. Taishi, and K. Hoshikawa, [J. Cryst. Growth](#) **556**, 125990 (2021).
- ⁷ E.G. Villora, K. Shimamura, Y. Yoshikawa, K. Aoki, and N. Ichinose, [J. Cryst. Growth](#) **270**, 420 (2004).
- ⁸ A.J. Green, J. Speck, G. Xing, P. Moens, F. Allerstam, K. Gumaelius, T. Neyer, A. Arias-Purdue, V. Mehrotra, A. Kuramata, K. Sasaki, S. Watanabe, K. Koshi, J. Blevins, O. Bierwagen, S. Krishnamoorthy, K. Leedy, A.R. Arehart, A.T. Neal, S. Mou, S.A. Ringel, A. Kumar, A. Sharma, K. Ghosh, U. Singiseti, W. Li, K. Chabak, K. Liddy, A. Islam, S. Rajan, S. Graham, S. Choi, Z. Cheng, and M. Higashiwaki, [APL Mater.](#) **10**, 029201 (2022).
- ⁹ A. Kyrtos, M. Matsubara, and E. Bellotti, [Appl. Phys. Lett.](#) **112**, 032108 (2018).
- ¹⁰ E. Ahmadi, O.S. Koksaldi, X. Zheng, T. Mates, Y. Oshima, U.K. Mishra, and J.S. Speck, [Appl. Phys. Express](#) **10**, 071101 (2017).
- ¹¹ A. Mauze, Y. Zhang, T. Itoh, F. Wu, and J.S. Speck, [APL Mater.](#) **8**, 021104 (2020).
- ¹² A. Mauze, Y. Zhang, T. Itoh, E. Ahmadi, and J.S. Speck, [Appl. Phys. Lett.](#) **117**, 222102 (2020).
- ¹³ N.K. Kalarickal, Z. Xia, J. McGlone, S. Krishnamoorthy, W. Moore, M. Brenner, A.R. Arehart, S.A. Ringel, and S. Rajan, [Appl. Phys. Lett.](#) **115**, 152106 (2019).
- ¹⁴ E. Ahmadi, O.S. Koksaldi, S.W. Kaun, Y. Oshima, D.B. Short, U.K. Mishra, and J.S. Speck, [Appl. Phys. Express](#) **10**, 041102 (2017).
- ¹⁵ S. Krishnamoorthy, Z. Xia, S. Bajaj, M. Brenner, and S. Rajan, [Appl. Phys. Express](#) **10**, 051102 (2017).
- ¹⁶ Z. Feng, A.F.M. Anhar Uddin Bhuiyan, M.R. Karim, and H. Zhao, [Appl. Phys. Lett.](#) **114**, 250601 (2019).
- ¹⁷ X. Du, Z. Li, C. Luan, W. Wang, M. Wang, X. Feng, H. Xiao, and J. Ma, [J. Mater. Sci.](#) **50**, 3252 (2015).
- ¹⁸ F. Alema, G. Seryogin, A. Osinsky, and A. Osinsky, [APL Mater.](#) **9**, 091102 (2021).
- ¹⁹ A. Hernandez, M.M. Islam, P. Saddatkia, C. Coddington, P. Dulal, S. Agarwal, A. Janover, S. Novak, M. Huang, T. Dang, M. Snure, and F.A. Selim, [Results Phys.](#) **25**, 104167 (2021).
- ²⁰ M. Baldini, M. Albrecht, A. Fiedler, K. Irmscher, R. Schewski, and G. Wagner, [ECS J. Solid State Sci. Technol.](#) **6**, Q3040 (2017).
- ²¹ S. Bin Anooz, R. Grüneberg, T.-S. Chou, A. Fiedler, K. Irmscher, C. Wouters, R. Schewski, M. Albrecht, Z. Galazka, W. Miller, J. Schwarzkopf, and A. Popp, [J. Phys. Appl. Phys.](#) **54**, 034003 (2021).
- ²² S. Lany, [APL Mater.](#) **6**, 046103 (2018).
- ²³ T. Kamimura, Y. Nakata, M.H. Wong, and M. Higashiwaki, [IEEE Electron Device Lett.](#) **40**, 1064 (2019).
- ²⁴ T.J. Asel, E. Steinbrunner, J. Hendricks, A.T. Neal, and S. Mou, [J. Vac. Sci. Technol. A](#) **38**, 043403 (2020).
- ²⁵ G. Hoffmann, Z. Cheng, O. Brandt, and O. Bierwagen, [APL Mater.](#) **9**, 111110 (2021).
- ²⁶ M. Higashiwaki, K. Sasaki, A. Kuramata, T. Masui, and S. Yamakoshi, [Phys. Status Solidi A](#) **211**, 21 (2014).
- ²⁷ K.M. Adkison, S.-L. Shang, B.J. Bocklund, D. Klimm, D.G. Schlom, and Z.-K. Liu, [APL Mater.](#) **8**, 081110 (2020).
- ²⁸ G. Hoffmann, M. Budde, P. Mazzolini, and O. Bierwagen, [APL Mater.](#) **8**, 031110 (2020).
- ²⁹ P. Vogt, F.V.E. Hensling, K. Azizie, C.S. Chang, D. Turner, J. Park, J.P. McCandless, H. Paik, B.J. Bocklund, G. Hoffman, O. Bierwagen, D. Jena, H.G. Xing, S. Mou, D.A. Muller, S.-L. Shang, Z.-K. Liu, and D.G. Schlom, [APL Mater.](#) **9**, 031101 (2021).
- ³⁰ Y.S. Kim, N. Bansal, C. Chaparro, H. Gross, and S. Oh, [J. Vac. Sci. Technol. Vac. Surf. Films](#) **28**, 271 (2010).
- ³¹ Y.-S. Kim, N. Bansal, and S. Oh, [J. Vac. Sci. Technol. Vac. Surf. Films](#) **28**, 600 (2010).
- ³² P. Mazzolini and O. Bierwagen, [J. Phys. Appl. Phys.](#) **53**, 354003 (2020).
- ³³ P. Mazzolini, A. Falkenstein, C. Wouters, R. Schewski, T. Markurt, Z. Galazka, M. Martin, M. Albrecht, and O. Bierwagen, [APL Mater.](#) **8**, 011107 (2020).
- ³⁴ P. Vogt, O. Brandt, H. Riechert, J. Lähnemann, and O. Bierwagen, [Phys Rev Lett](#) **119**, 196001 (2017).
- ³⁵ P. Mazzolini, P. Vogt, R. Schewski, C. Wouters, M. Albrecht, and O. Bierwagen, [APL Mater.](#) **7**, 022511 (2019).
- ³⁶ P. Mazzolini, A. Falkenstein, Z. Galazka, M. Martin, and O. Bierwagen, [Appl. Phys. Lett.](#) **117**, 222105 (2020).
- ³⁷ Y.-S. Kim, N. Bansal, and S. Oh, [J. Vac. Sci. Technol. Vac. Surf. Films](#) **29**, 041505 (2011).

Supplementary material to “Towards controllable Si-doping in oxide molecular beam epitaxy using a solid SiO source: Application to β -Ga₂O₃”

Amorphous SiO₂ growth for SiO flux calibration

The amorphous SiO₂ layer was deposited on a 2” (0001) Al₂O₃ substrate at a $T_{SiO} = 1000$ °C under conditions that provide full incorporation of SiO flux, i.e., a substrate temperature $T_{sub}=100$ °C, an oxygen flux of 1 standard cubic centimeter per minute (sccm), an RF plasma power $P_{RF} = 250$ W. The growth rate was calculated as ratio of film thickness (12 nm, measured ex-situ by X-ray reflectometry, Fig. S1) and growth time of 8 minutes. By using the mass density of amorphous SiO₂ ($\rho_{SiO_2} = 2.2$ g/cm³) and the SiO₂ atomic mass ($M_{SiO_2} = 60$ amu) we can calculate the density of SiO₂ molecules N_{SiO_2} using the following formula:

$$N_{SiO_2} = \frac{\rho_{SiO_2} N_A}{M_{SiO_2}}, \quad (S1)$$

where N_a is Avogadro’s constant. Multiplying N_{SiO_2} by GR_{SiO_2} , we obtained the silicon flux (Φ_{Si}) at 1000°C for the SiO source:

$$\Phi_{SiO}^{1000^\circ C} = GR_{SiO_2} N_{SiO_2} = 5.5 \cdot 10^{13} \text{ cm}^{-2}. \quad (S2)$$

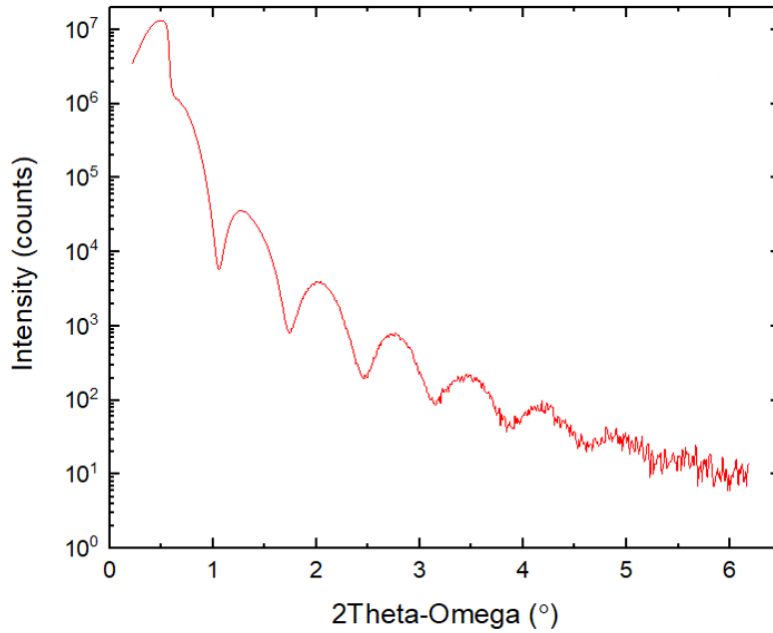


Figure S1: XRR curve for a 12nm thick amorphous SiO₂ layer.

Growth details for β -Ga₂O₃

The growth of the homoepitaxial samples was performed on diced 5 x 5 mm² pieces of Fe-doped β -Ga₂O₃ semi-insulating substrates (Novel Crystal Technology) close to stoichiometric conditions (Ga beam equivalent pressure $BEP_{Ga} = 3.48 \times 10^{-7}$ mbar, O -flux = 1 sccm, $P_{RF} = 250$ W), at $T_g = 750$ °C. The same growth conditions were applied for (-201)-oriented growth on 2" (0001) Al₂O₃ substrates with the only exception of a lower substrate temperature ($T_g = 550$ °C) due to the orientation dependent GR in β -Ga₂O₃ by MBE,^{33,38} and the initial growth of a nucleation layer (about 15-30 nm thick, $P_{RF} = 400$ W).

SiO source oxidation model

In order to physically understand the oxidation process than occurs at the SiO surface, when active oxygen is supplied, we analyzed the Si SIMS profiles as a function of the T_{SiO} of several β -Ga₂O₃ layers. A simple oxidation model was then formulated to tentatively describe the oxidation process. Considering a fixed probability that a certain percentage of our source surface will further oxidize into SiO₂, as a function of T_{SiO} and the oxygen background pressure in the MBE chamber, we expect an exponential decay of the accessible SiO surface, and hereby of the SiO flux. A simple sketch that explain the process is shown in Figure S2.

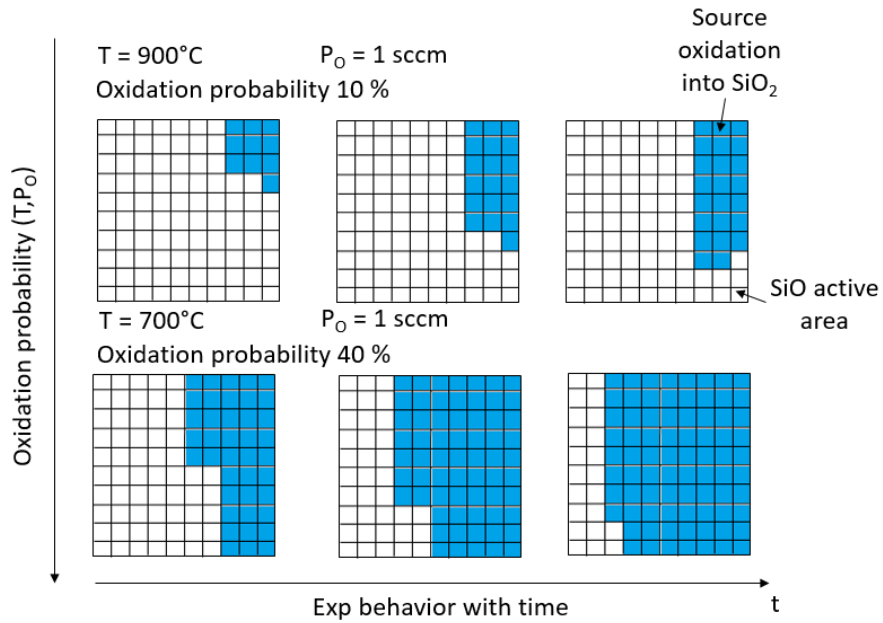


Figure S2 Example of the oxidation process that may take place on our source as a function of T_{SiO} and oxygen background pressure. In this case the oxygen pressure is fixed.

Transport measurement

Van-der-Pauw-Hall measurements were performed at a current of 100 μA and a magnetic field of $B = \pm 0.7\text{ T}$ oriented perpendicularly to the substrate surface. Prior to measurement, 20 nm Ti/ 20 nm Pt/ 100 nm Au circular contacts were deposited by electron-beam evaporation in the corners of the square sample through a shadow mask and confirmed to be ohmic without annealing by current-voltage measurements.